Refractive indices for molecular crystals from the response of X-ray constrained Hartree–Fock wavefunctions†

Dylan Jayatilaka,*[a] Parthapratim Munshi,[a] Michael J. Turner,[b] Judith A. K. Howard[b] and Mark A. Spackman*[a]

Received 26th March 2009, Accepted 11th May 2009
First published as an Advance Article on the web 10th June 2009
DOI: 10.1039/b906072c

Refractive indices for molecular crystals are obtained from Hartree–Fock wavefunctions constrained to reproduce a set of experimental X-ray structure factors. Coupled-perturbed Hartree–Fock theory is used to calculate the in-crystal effective polarizabilities from which the refractive indices are obtained, thus eliminating the need for the calibration procedure used in earlier work by Whitten *et al.* [*J. Chem. Phys.* 2006, **125**, 174505]. The results clearly demonstrate that these X-ray constrained Hartree–Fock (XCHF) wavefunctions reflect genuine effects of intermolecular interactions in crystals. Molecular dipole moments are consistently in excellent agreement with *ab initio* MP2 estimates that incorporate the effects of the crystal field. Consistent agreement of the XCHF refractive indices with experimental measurements at optical frequencies confirms that this approach can provide both meaningful results and considerable insight into the relative importance of molecular properties and crystal field effects in determining the detailed nature of the refractivity tensor.

1. Introduction

Molecular crystals show some promise for non-linear optical (NLO) applications.[1] The first step on the path to engineering desired NLO properties in molecular crystals is the ability to understand and predict linear optical properties, *e.g.* the refractive index, which depends on the in-crystal molecular polarizability. However, predicting even the linear optical properties for molecular crystals is quite challenging because one must account for the intermolecular interactions which occur in the crystal, as well as electron correlation effects which may be intra- or intermolecular in nature.

To overcome these challenges we have recently proposed to use Hartree–Fock (HF) wavefunctions constrained to reproduce the structure factor magnitudes from accurate X-ray diffraction measurements on molecular crystals.[2] Since these structure factors are essentially the Fourier components of the electron density, they reflect the actual correlation and intermolecular interaction effects present in the real crystal; hence a wavefunction constrained to reproduce these structure factors will also include these same effects. We have shown that the refractive indices for a few simple molecular crystals can indeed be predicted well from these constrained wavefunctions.[2] However, this success was achieved using a scaling procedure and an approximate formula for the polarizability.

In this paper we improve upon the previous treatment by using coupled-perturbed Hartree–Fock (CPHF) theory to obtain the effective polarizabilities from the X-ray constrained wavefunction. In this way the scaling procedure used previously is entirely avoided and the same formula for calculating the *ab initio* polarizabilities is used to calculate the in-crystal effective polarizabilities. The theory for calculating refractive indices from in-crystal molecular polarizabilities is presented in the next section, followed by a detailed discussion of results for benzene and five dipolar molecules of relevance to NLO studies.

2. Estimating the local electric field

2.1 Refractive index, polarization, and susceptibility in molecular crystals

In linear optics the refractive indices $\boldsymbol{n}$ and the optic axes of a molecular crystal are obtained from the eigenvalues and eigenvectors of $\boldsymbol{\varepsilon}^{1/2}$, respectively. The permittivity tensor $\boldsymbol{\varepsilon}$ gives the polarization or dipole moment density $\boldsymbol{P}$ induced in a *bulk* sample due to an applied electric field $\boldsymbol{E}$,

$$\boldsymbol{P} = \varepsilon_0(\boldsymbol{\varepsilon} - \mathbf{1})\boldsymbol{E} = \varepsilon_0\boldsymbol{\chi}\boldsymbol{E} \quad (1)$$

Here, ε_0 is the permittivity of free space and the dielectric susceptibility tensor is $\boldsymbol{\chi} = \boldsymbol{\varepsilon} - \mathbf{1}$. On the other hand, when a field $\boldsymbol{F}$ is applied to a *molecule* it develops an induced dipole moment

$$\Delta\boldsymbol{\mu} = \boldsymbol{\alpha}\boldsymbol{F} \quad (2)$$

Here $\boldsymbol{\alpha}$ is the molecular dipole polarizability tensor. Since $\boldsymbol{P}$ is an induced dipole moment density, a comparison of eqns (1)

[a] *Chemistry-M313, School of Biomedical, Biomolecular & Chemical Sciences, University of Western Australia, Crawley WA 6009, Australia. E-mail: dylan.jayatilaka@uwa.edu.au, mark.spackman@uwa.edu.au*
[b] *Department of Chemistry, University of Durham, South Road, Durham, UK DH1 3LE*

† Electronic supplementary information (ESI) available: Crystallographic details for X-ray diffraction data and complete polarizability tensors for all molecules (HF, MP2, MP2 + field and XCHF). See DOI: 10.1039/b906072c

and (2) suggests that the susceptibility and polarizability are related. Suppose we have a molecular crystal composed of k identical molecules in the unit cell. Then the total dipole moment density in the unit cell is a sum of molecular dipole moment densities

$$\boldsymbol{P} = \sum_k \boldsymbol{P}_k = \sum_k \frac{\Delta \boldsymbol{\mu}_k}{V} \tag{3}$$

where V is the volume of the unit cell. Substituting eqn (2) for the polarizabilities $\boldsymbol{\alpha}_k$ of each of the molecules k in the unit cell, and removing a factor ε_0, gives

$$\boldsymbol{P} = \varepsilon_0 \sum_k \frac{\boldsymbol{\alpha}_k}{\varepsilon_0 V} \boldsymbol{F} = \varepsilon_0 \sum_k \boldsymbol{a}_k \boldsymbol{F}. \tag{4}$$

Assuming that the field $\boldsymbol{F}$ experienced by each molecule is the same as the field $\boldsymbol{E}$ applied to the crystal, a comparison of the equation above with eqn (1) gives

$$\boldsymbol{\chi} = \sum_k \boldsymbol{a}_k. \tag{5}$$

In eqn (4) we have defined the dimensionless reduced polarizability

$$\boldsymbol{a}_k = \frac{\boldsymbol{\alpha}_k}{\varepsilon_0 V} \tag{6}$$

which gives the polarization of each molecule

$$\boldsymbol{P}_k = \varepsilon_0 \boldsymbol{\alpha}_k \boldsymbol{F}. \tag{7}$$

Note that the molecules in the unit cell are all related by symmetry so that the polarizabilities $\boldsymbol{\alpha}_k$ are related by symmetry.

2.2 Local field theory for the dielectric susceptibility

Eqn (5) is a poor approximation for $\boldsymbol{\chi}$ since the field $\boldsymbol{F}$ experienced by each molecule in the crystal is not necessarily the same as the field $\boldsymbol{E}$ applied to the crystal. Induced charges and induced dipoles on neighbouring molecules and on the surface of the crystal lead to electric fields in addition to the field $\boldsymbol{E}$ applied to the crystal. To treat this local field we follow Dunmur[3] and Bounds and Munn,[4] and assume that the local field appears only because of induced dipoles distributed at various sites throughout the molecule *i.e.* if the field at site A in molecule k is written as $\boldsymbol{F}_{kA}$, then the polarization at that same site is given by (*cf.* eqn (7)),

$$\boldsymbol{P}_{kA} = \varepsilon_0 \boldsymbol{\alpha}_{kA} \boldsymbol{F}_{kA} \tag{8}$$

where $\boldsymbol{a}_{kA}$ is the dimensionless reduced polarizability for site A in molecule k (*cf.* eqn (6)). Then it can be shown that the susceptibility is given by

$$\boldsymbol{\chi} = \sum_{kA,lB} \boldsymbol{a}_{kA} (\mathbf{1} - \mathbf{La})^{-1}_{kA,LB} \tag{9}$$

Here, $\mathbf{a}$ is a $3N \times 3N$ block diagonal matrix whose 3×3 diagonal blocks are the site polarizabilities $\boldsymbol{a}_{kA}$. $\mathbf{L}$ is the dimensionless $3N \times 3N$ Lorentz factor tensor, comprised of 3×3 blocks $\boldsymbol{L}(\boldsymbol{r}_{kA},\boldsymbol{r}_{lB})$. The product $\boldsymbol{L}(\boldsymbol{r}_{kA},\boldsymbol{r}_{lB})\boldsymbol{a}_{lB}\boldsymbol{F}_{lB}$ yields the electric field at $\boldsymbol{r}_{kA}$ due to all the induced dipoles translationally equivalent to the induced moment at $\boldsymbol{r}_{lB}$ which has magntitude $\varepsilon_0 V \boldsymbol{a}_{lB}\boldsymbol{F}_{lB}$. The 3×3 Lorentz factor tensor involves a lattice summation. Formulas for $\boldsymbol{L}(\boldsymbol{r}_{kA},\boldsymbol{r}_{lB})$ are available and are easily evaluated (see ref. 5 and appendix B of ref. 6). The notation $\mathbf{M}^{-1}_{kA,lB}$ in eqn (9) means to take the (kA,lB)-th 3×3 submatrix of the $3N \times 3N$ supermatrix $\mathbf{M}^{-1}$ (*i.e.* invert first, then take the submatrix).

According to eqn (9), the refractive indices and optic axes of the molecular crystal depend on the in-crystal site dipole polarizabilities and the corresponding local field factor tensors. Comparing this equation with the naive one, eqn (5), we see that they are nearly the same except for the presence of the inverse matrix which modifies the external field to give the local field experienced at each site. To obtain the site polarizabilities we previously employed several approximations to eqn (9):[2]

- In the anisotropic Lorentz field factor approximation (ALFFA), the dipole local field factor tensor $\boldsymbol{L}$ is replaced by one-third the identity matrix and the molecular polarizability is used. It does not matter where the polarizability is located, as the $\boldsymbol{L}$ are independent of this choice. This yields essentially the Clausius-Mossotti formula.
- The RLFT1 model, where the dipole induced in the molecule is situated at the centre of mass.
- The RLFTn model, where the Lorentz tensor is averaged over the n positions of the non-hydrogen atoms in a molecule, and eqn (9) is subsequently used with a single dimensionless polarizability, eqn (6), per molecule.

In ref. 2 we concluded that the RLFT1 model is inappropriate for large molecules, especially those anisotropic in shape, and of these three approximations RLFTn refractive indices were in best agreement with experiment. For that reason all results we discuss in the present work have been obtained using the RLFTn approximation.

2.3 Effective dipole moments and polarizabilities by X-ray constrained wavefunctions

To use eqn (9) we must be able to estimate the dipole moment and polarizabilities in the molecular crystal, and this is now described. The permanent electronic dipole moment of a molecule is given in atomic units by

$$\boldsymbol{\mu} = \int \rho(\boldsymbol{r}) \mathrm{d}\boldsymbol{r}. \tag{10}$$

In the restricted Hartree–Fock (RHF) approximation the electron charge density $\rho(\boldsymbol{r})$ is given in terms of the density matrix $\boldsymbol{D}$ and a set of real basis functions $\{g_a\}$ as

$$\rho(\boldsymbol{r}) = -\sum_{ab} D_{ab} g_a(\boldsymbol{r}) g_b(\boldsymbol{r}) \tag{11}$$

$\boldsymbol{D}$ depends on the occupied HF molecular orbital (MO) coefficients $\boldsymbol{c}_O$,

$$\boldsymbol{D} = 2\boldsymbol{c}_O \boldsymbol{c}_O^T. \tag{12}$$

Unlike an RHF calculation, the occupied MO's are here obtained using a constrained Hartree–Fock procedure by minimising the Hartree–Fock energy and an additional residual χ^2,

$$\chi^2 = \frac{1}{N_{\mathrm{obs}} - N_{\mathrm{var}}} \sum_k \frac{(F_k^{\mathrm{calc}} - F_k^{\mathrm{obs}})^2}{\sigma_k^2}, \tag{13}$$

which expresses the deviation of the calculated electron density structure factors F_k^{calc} from the observed ones F_k^{obs}, accurate to within experimental error σ_k. The quantity minimized is $E_{\mathrm{HF}} + \lambda\chi^2$, where E_{HF} is the usual Hartree–Fock energy and λ is a Lagrange multiplier that gives the fit to the X-ray diffraction data more or less influence. The minimisation of this energy expression leads to occupied MO's which simultaneously minimise E_{HF} and reproduce the experimental electron density structure factors. This X-ray constrained HF (XCHF) method has been applied to several systems for reconstructing the electron density (see, *e.g.* ref. 7). Here it is used to obtain an experimentally derived electron density ρ to calculate an in-crystal electronic dipole moment *i.e.* a dipole moment that includes the effects of interactions, electrostatic or otherwise, from all the surrounding molecules.

Using definitions (2) and (10), the in-crystal electronic polarizability is a field derivative of the permanent electronic dipole moment,

$$\alpha_{\alpha\beta} = \int \rho^{\beta} r_{\alpha}\, \mathrm{d}\boldsymbol{r} \tag{14}$$

where $\rho^{\beta} = \partial\rho/\partial F_{\beta}$. On the other hand, (11) implies that

$$\rho^{\beta} = -\sum_{ab} D_{ab}^{\beta} g_a(\boldsymbol{r}) g_b(\boldsymbol{r}) \tag{15}$$

where $D_{ab}^{\beta} = \partial D_{ab}/\partial F_{\beta}$ is the derivative density matrix. Substituting this in (14) gives the polarizability in terms of standard dipole matrix elements,

$$\rho^{\beta} = -\sum_{ab} D_{ab}^{\beta} \langle g_a | r_{\alpha} | g_b \rangle. \tag{16}$$

$\boldsymbol{D}^{\beta}$ is obtained by solving the CPHF equations. These equations are usually written in terms of the $\bar{\boldsymbol{U}}^{\beta}$ matrices,[8,9] defined by

$$\frac{\partial \boldsymbol{c}_O}{\partial F_{\beta}} = \boldsymbol{c}_O^{\beta} = \boldsymbol{c}_V \bar{\boldsymbol{U}}^{\beta} \tag{17}$$

where $\boldsymbol{c}_V$ are the columns of virtual (or unoccupied) MO coefficients. $\bar{\boldsymbol{U}}^{\beta}$ is of dimension $n_V \times n_O$ where n_V is the number of virtual MO's and n_O the number of occupied MO's. The $\bar{\boldsymbol{U}}^{\beta}$ satisfy the linear CPHF equations

$$\boldsymbol{H}\bar{\boldsymbol{U}}^{\beta} = \bar{\boldsymbol{\mu}}^{\beta} \tag{18}$$

where $\bar{\mu}_{AI}^{\beta} = \langle \phi_A | \mu_{\beta} | \phi_I \rangle$ are virtual-occupied MO dipole matrix elements and $\boldsymbol{H}$ is a supermatrix involving orbital energies and two-electron integrals[8,10] (for a modern and brief treatment see, *e.g.*, ref. 11, eqn (4)). Note that for constrained HF calculations the $\boldsymbol{H}$ matrix takes its usual form (*i.e.* it is defined in terms of two electron integrals in the X-ray constrained MO basis, and the eigenvalues are the diagonal elements of the usual Fock matrix in the constrained MO basis). We do not include any contributions which come from the field derivatives of the X-ray structure factors, since we do not have access to that information. From eqns (12) and (17), the derivative density matrix is given in terms of the $\bar{\boldsymbol{U}}^{\beta}$ by

$$\boldsymbol{D}^{\beta} = 2\boldsymbol{c}_V \bar{\boldsymbol{U}}^{\beta} \boldsymbol{c}_O^{T} + 2\boldsymbol{c}_O (\bar{\boldsymbol{U}}^{\beta})^{T} \boldsymbol{c}_V^{T} \tag{19}$$

Hence the refractive indices can be evaluated *via* (9) using (16) and the above equation.

In general, the polarizability is not purely electronic as assumed here, but has contributions from the perturbation of the nuclear charge distribution by the local field, the so-called vibrational polarizability. There is also an important frequency dependence to the polarizability. The vibrational polarizability is expected to be small at optical frequencies since the nuclei are too heavy to respond to oscillating electric fields at optical frequencies. The problem of frequency dependence may be mitigated by extrapolating experimental refractive indices to zero frequency, but this is only possible where experimental measurements of refractive indices have been made at a sufficient number of wavelengths. Even where such measurements have been made, extrapolation to zero frequency can be problematic and involve significant uncertainty. For this reason we compare the present zero-frequency XCHF results with experimental measurements at the longest wavelength available, bearing in mind that the static XCHF values should lie below the experimental values at any optical frequency.

3. Results and discussion

3.1 Calculation details

As illustrative examples we have applied our approach to benzene (space group *Pbca*), urea ($P\bar{4}2_1m$), and MNA (*Ia*), which were also examined in our previous paper,[2] where details of those X-ray data have been fully described. In addition, we have measured new X-ray diffraction data at 100 K on three important organic NLO materials: POM ($P2_12_12_1$), NPP and PNP (both $P2_1$), as well as the archetype donor–acceptor molecule *p*-nitroaniline (*p*NA, $P2_1/c$). (Table S1 of the ESI† summarizes relevant details of the X-ray diffraction data). Molecular structures of the dipolar molecules are given in Fig. 1. Unlike our previous work,[2] where wavefunction fitting was performed with a DZP basis set,[12] here we use the DZP+ basis set[13] for the XCHF calculations, because the polarizabilities obtained with addition of diffuse functions are much closer to the Hartree–Fock limit. This basis set provides a link with our earlier work using the DZP basis set, but it is smaller than most common basis sets optimized for polarizability calculations (*e.g.*, those constructed by Sadlej[14]). This is an important consideration for the larger molecules pursued in this study, especially in view of the convergence difficulties often encountered in the present calculations; section 4 addresses this in more detail. The XCHF calculations used the formalism for noncentrosymmetric crystals described in ref. 7, with no corrections made for extinction or anomalous dispersion.

As described above, the constrained wavefunction is consistent with the observed structure factors to an accuracy dictated by the multiplier λ, which must be determined for each molecule. Fitting was pursued by increasing λ until the weighted residual $R_{\mathrm{w}}(F)$ from the XCHF calculation approaches that achieved in a multipole refinement against the same set of diffraction data. Details of the constrained wavefunction refinements are presented in Table 1. For benzene and urea the value of λ used to obtain a given level of fit for these larger basis sets is less than that required for the

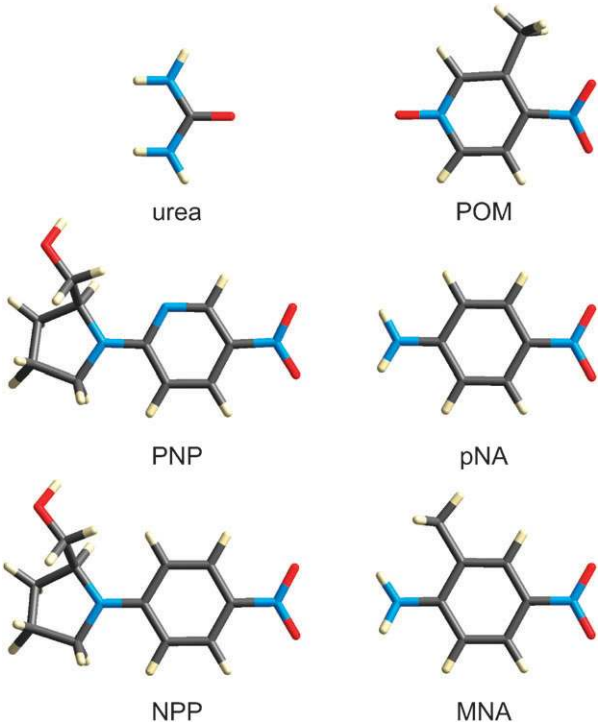

Fig. 1 Dipolar molecules studied in this work. The molecules are all drawn to the same scale, with the charge transfer axis along the horizontal direction. POM = 3-methyl-4-nitropyridine-*N*-oxide; PNP = 2-(*N*-(L)-prolinol)-5-nitropyridine; NPP = *N*-4-nitrophenyl-L-prolinol; pNA = 4-nitroaniline; MNA = 2-methyl-4-nitroaniline.

Table 1 Refinement indices for multipole refinement and X-ray constrained Hartree–Fock (XCHF) fits to diffraction data

		χ^2	$\%R(F)$	$\%R_w(F)$
Benzene	Multipole refinement	1.08	1.89	1.69
	XCHF $\lambda = 0.00$	2.72	2.70	2.77
	XCHF $\lambda = 0.250$	1.01	1.85	1.69
Urea	Multipole refinement	2.46	1.17	0.64
	XCHF $\lambda = 0.00$	16.84	1.81	1.73
	XCHF $\lambda = 0.110$	2.29	1.17	0.64
POM	Multipole refinement	3.94	2.23	1.84
	XCHF $\lambda = 0.00$	8.88	2.90	2.57
	XCHF $\lambda = 0.170$	4.54	2.28	1.84
NPP	Multipole refinement	1.82	1.62	1.23
	XCHF $\lambda = 0.00$	4.10	2.21	1.93
	XCHF $\lambda = 0.575$	1.69	1.64	1.24
PNP	Multipole refinement	2.16	1.22	1.11
	XCHF $\lambda = 0.00$	5.81	1.90	1.92
	XCHF $\lambda = 0.385$	2.01	1.25	1.13
pNA	Multipole refinement	3.50	2.47	2.04
	XCHF $\lambda = 0.00$	7.14	3.30	3.00
	XCHF $\lambda = 0.770$	3.38	2.51	2.06
MNA	Multipole refinement	2.17	1.74	1.59
	XCHF $\lambda = 0.00$	3.70	2.28	2.16
	XCHF $\lambda = 2.20$	1.88	1.69	1.54

DZP basis. This was noticed before[15] and is most likely due to the fact that the extra polarization functions allow the molecular wavefunction to more readily distort into the form that best reproduces the crystalline electron density.

For comparison with XCHF results we have also performed a series of *ab initio* calculations for each molecule with Gaussian03,[16] using the same DZP+ basis set, geometries and coordinate systems. These calculations represent an attempt to explore the effects of electron correlation and the electric field due to surrounding molecules in the crystal. Tables 2 and 3 present results obtained at the Hartree–Fock and MP2 levels of theory, and also MP2+field, where an electric field has been applied to the molecules, the field being obtained in a self-consistent manner using dipole lattice sums (*i.e.* the Lorentz factor tensor formalism[5]) and MP2 dipole moments in an iterative fashion.[17]

3.2 Molecular dipole moments

XCHF molecular dipole moment magnitudes and directions are compared with the results from the *ab initio* calculations in Table 2. For all molecules we see the expected decrease in μ on inclusion of electron correlation, and subsequent enhancement with the application of a Lorentz field. From the *ab initio* calculations dipole moment enhancements are predicted to be substantial at the MP2 level, and in the range 27–28% (for NPP and PNP) to 62% (for MNA). These factors are greater than previous estimates obtained at the Hartree–Fock level with a 6-31++G(d,p) basis set, which were in the range 15–16% (NPP and PNP) to 42% (MNA), a result which seems to be almost entirely due to the overestimate of the zero-field dipole moment at the Hartree–Fock level in ref. 17. Of more importance to our present goals are the XCHF results and their remarkable agreement with the MP2+field values. The results in Table 2 labelled "Experiment" are from measurement in the gas phase (for urea) or in dilute solution, and the MP2+field and XCHF results are systematically larger, in many cases by a substantial amount. We are led to conclude that despite the fact that the XCHF wavefunctions are only single determinant and minimize the Hartree–Fock energy, the additional constraint of fitting the X-ray structure factors results in a wavefunction that reflects the effects of both electron correlation and intermolecular interactions (*i.e.* hydrogen bonding and the crystalline electric field experienced by the molecule). It is also worth noting that the constraints imposed by a single determinant wavefunction prevent dipole moment estimates from becoming exaggerated, something that has been shown to be a common deficiency of many multipole refinements.[18]

The magnitude and direction of the Lorentz field computed at the MP2 level using the RLFT*n* approximation shed considerable insight into the origin of the dipole moment enhancements. At 8.29 GV m^{-1} the Lorentz field for urea is extremely large and directed along the molecular twofold axis. The magnitude also agrees well with the value of 8.59 GV m^{-1} reported by Reis, Papadopoulos and Munn[19] from a similar computational approach, also at the MP2 level. The largest discrepancies between XCHF and MP2+field results in Table 2 are observed for POM and MNA, where we expect that the Lorentz field is a poor approximation to the actual crystal electric field experienced by these molecules. In

Table 2 Molecular dipole moments from wavefunction fitting to X-ray diffraction data (XCHF) compared with *ab initio* results. μ is the magnitude of the dipole moment (in Debye) and θ the angle between the dipole moment and the charge transfer axis for the molecule.[a] F is the magnitude of the Lorentz field (in GV m^{-1}) and θ_F the angle it makes with the charge transfer axis of each molecule

		HF	MP2	MP2 + field	XCHF	Experiment
Urea	μ	5.11	4.61	6.51	6.89	3.83(4)[b]
	θ	0	0	0	0	
	F, θ_F			8.29, 0°		
POM	μ	1.04	0.82	1.32	0.73	0.69(5)[c]
	θ	110	82	131	82	
	F, θ_F			0.76, 175°		
NPP	μ	7.52	6.82	8.70	8.99	7.3(5)[d]
	θ	4	4	3	5	
	F, θ_F			1.13, 17°		
PNP	μ	6.65	6.07	7.71	7.66	7.2(6)[e]
	θ	18	18	20	22	
	F, θ_F			1.30, 45°		
pNA	μ	7.90	6.96	10.90	11.12	6.2(6),[f] 6.81(7),[g] 7.4,[h] 7.62[i]
	θ	1	1	2	9	
	F, θ_F			4.42, 12°		
MNA	μ	8.30	7.35	11.90	9.20	7.4(2),[e] 6.4,[j] 7.0,[k] 6.2[l]
	θ	3	4	4	−1	
	F, θ_F			4.73, 13°		

[a] Charge transfer axes are along the C═O direction for urea and the N···NO_2 direction for the remaining molecules (see Fig. 1). [b] In the gas phase.[20] Measurements for urea in solution are numerous and lie in the range 4.20–6.38 D; Table S9 of ref. 21 provides a full compilation. [c] In benzene.[22] [d] In chloroform.[23] [e] In dioxane.[24] [f] In acetone.[25] [g] In toluene.[26] [h] In dioxane.[27] [i] In benzene.[28] [j] In benzene.[29] [k] In dioxane.[29] [l] In dioxane.[25]

addition, the small dipole moment for POM arises from the vector sum of large contributions from the various functional groups around the ring.[17] Evidence of this is clearly seen in the variation of the dipole moment direction by almost 50° for the various methods in Table 2. The Lorentz field for NPP and PNP is relatively modest, and directed close to the charge transfer axis for NPP, but at 45° from this axis for PNP. For both pNA and MNA the Lorentz field is quite large and closely aligned with the molecular charge transfer axes, a combination directly responsible for the large dipole moment enhancements observed in the MP2 + field calculations.

3.3 Molecular polarizabilities

Polarizability tensors for molecules depend on the coordinate system chosen for their computation and, with the exception of benzene and urea, there are no obvious choices for the molecules under investigation. For that reason we report all elements of these tensors, as well as mean polarizabilities and polarizability anisotropies, in Table S2 of the ESI,† and discuss only a few specific details here. Considering the *ab initio* calculations first, we observe an expected increase in mean polarizability with the inclusion of electron correlation, in the range of 8–10% for most molecules, but the effect is quite modest (~1%) for benzene. In all cases the MP2 polarizability anisotropy is greater than that at the HF level. Comparison of MP2 + field and MP2 (zero field) results reveals that the effect of the crystal field on the polarizability is very small for urea (despite the large Lorentz field applied, as noted previously in ref. 19) and POM, of the order of +1% for NPP and PNP, but considerably larger at +6% for pNA and MNA. For benzene we may compare the principal polarizabilities with those obtained experimentally in the gas phase. The experimental results measured at 632.8 nm are (44.9 ± 1.3, 82.7 ± 1.0, 82.7 ± 1.0) au,[30] compared with our XCHF result of (42.9, 80.6, 81.6) au, (41.0, 80.3, 80.5) au for the MP2 wavefunction and (41.4, 78.7, 78.9) at the HF level. As observed for the dipole moments, these results strongly suggest that the XCHF wavefunction includes crystalline environment effects as well as electron correlation effects.

3.4 Crystal refractive indices

Our main objective in this study was to obtain molecular polarizabilities from the response of XCHF wavefunctions for the purpose of computing crystal refractive indices. In this manner we can meaningfully compare the outcomes of the wavefunction fitting procedure with experimental measurements, something which is impossible to do for the polarizability itself (with the possible exception of benzene). Since the refractive index is a function of the number density of particles, we calculate all refractive indices using cell dimensions observed at room temperature (see Table S1),† and the molecular polarizabilities derived from X-ray diffraction measurements at 100 K are used for the XCHF calculations. Table 3 compares XCHF refractive indices with those based on HF, MP2 and MP2 + field *ab initio* polarizability calculations, all based on the RLFT*n* local field treatment, and also with experimental measurements. We discuss results for each molecular crystal in turn, bearing in mind that the XCHF results refer to zero frequency, and are

Table 3 Principal crystal refractive indices from wavefunction fitting to X-ray diffraction data (XCHF) compared with results obtained from *ab initio* wavefunctions. The principal components are labelled in order $n_X \leq n_Y < n_Z$,[33] and for benzene and POM (both orthorhombic) and urea (tetragonal) they coincide with the unit cell axes. For NPP, PNP, pNA and MNA (all monoclinic) one principal axis (n_Y in all cases) coincides with the cell *b* axis, and the other two lie in the *ac* plane, the largest of them (n_Z) making an angle θ with the *a* axis. All results have been obtained using the RLFT*n* approximation

		Hartree–Fock	MP2	MP2 + field	XCHF	Experiment
Benzene	$n_X = n_c$	1.501	1.506			1.550[a]
	$n_Y = n_a$	1.520	1.527		1.543	1.544[a]
	$n_Z = n_b$	1.621	1.635		1.639	1.646[a]
Urea	$n_X = n_Y = n_a = n_b$	1.385	1.441	1.446	1.450	1.477[b]
	$n_Z = n_c$	1.522	1.615	1.593	1.595	1.583[b]
POM	$n_X = n_a$	1.553	1.580	1.579	1.553	1.625[c]
	$n_Y = n_c$	1.582	1.623	1.620	1.600	1.663[c]
	$n_Z = n_b$	1.708	1.821	1.810	1.777	1.829[c]
NPP	n_X	1.420	1.445	1.444	1.451	1.457[d]
	$n_Y = n_b$	1.627	1.689	1.695	1.674	1.774[d]
	n_Z	1.711	1.799	1.819	1.793	1.926[d]
	θ	43	43	43	42	
PNP	n_X	1.427	1.454	1.453	1.434	1.456[e]
	$n_Y = n_b$	1.615	1.681	1.686	1.614	1.732[e]
	n_Z	1.703	1.804	1.815	1.735	1.880[e]
	θ	41	41	41	40	
pNA	n_X	1.421	1.443	1.441	1.423	1.525(2),[f] 1.556[g]
	$n_Y = n_b$	1.624	1.672	1.686	1.633	1.756(3),[f] 1.78[g]
	n_Z	1.750	1.832	1.930	1.974	1.788(4),[f] 2.01[g]
	θ	47	48	50	52	
MNA	n_X	1.413	1.422	1.418	1.464	1.441(2),[h] 1.35[i]
	$n_Y = n_b$	1.639	1.688	1.699	1.661	1.732(3),[h] 1.51[i]
	n_Z	1.787	1.878	2.010	1.849	2.063(6),[h] 1.76[i]
	θ	27	27	27	28	

[a] Measurements at 588 nm.[31] [b] Computed at 1064 nm from Sellmeier equation in ref. 32; extrapolation to zero frequency gives values of 1.472 and 1.579. [c] Measurements at 1063.2 nm.[34] [d] Measurements at 1064 nm.[35] [e] Measurements at 1064 nm.[36] [f] Measurements at 588 nm;[37] no assignment of directions is given in the original publication. [g] Measurements at 588 nm; see ref. 38 for a detailed discussion. [h] Measurements at 1064 nm.[39] [i] Computed at 1064 nm from Sellmeier equation in ref. 40; extrapolation to zero frequency gives values of 1.68, 1.47 and 1.34.

expected to lie below the experimental measurements obtained at optical frequencies.

3.4.1 Benzene. The refractive indices for crystalline benzene have only been measured at a single wavelength, and it is not clear that the assignment of n_a and n_c is definitive. Nevertheless, XCHF results are slightly lower than those of Gay and Lemanceau[31] measured at 588 nm, and the agreement of XCHF with experiment is significantly better than that seen for MP2 or HF polarizabilities, providing additional evidence that the wavefunction constraint is modifying the HF wavefunction to reflect genuine features of the molecule in the crystal.

3.4.2 Urea. The experimental refractive indices for urea have been derived from measured angle tuning curves for type I second harmonic generation, and Halbout *et al.* reported only a modified Sellmeier fit to their results[32] (*i.e.*, no actual measurements were reported at specific frequencies). Their result for $n_a = n_b$ also agrees with the value of 1.48 derived from the Sellmeier fit reported by Betzler *et al.*,[41] and XCHF, MP2 + field, MP2 and HF results in Table 3 all lie suitably below this. However, the best *ab initio* estimates of n_c, as well as the XCHF result, are greater than the experimental result of 1.583, an anomaly that has also been noted by Reis *et al.*,[19] whose HF and MP2 results from a similar approach are consistent with those in Table 3. We note with interest that the effect of a Lorentz field on the MP2 calculations is small, but leads to remarkably good agreement with the XCHF results.

3.4.3 POM. We can see from Table 3 that the effect of electron correlation is significant, increasing all principal refractivities, especially n_b which increases by almost 7%. Addition of the Lorentz field has an extremely small effect, reflecting the very small field magnitude, 0.76 GV m^{-1}. XCHF results are in remarkably good agreement with the experimental measurements of Zyss *et al.*,[34] on average only 3–4% below those measurements made at 1063.2 nm. In contrast, we note that a semiempirical TDHF/AM1 approach using a combination of cluster calculations and a multiplicative scheme underestimates the same experimental measurements by 11–14%.[42]

3.4.4 NPP and PNP. Electron correlation increases the principal refractive indices by 2%–6% for both NPP and PNP, and as observed for POM, the effect of the small Lorentz field (1.13 and 1.30 GV m^{-1}, respectively) is modest. XCHF results

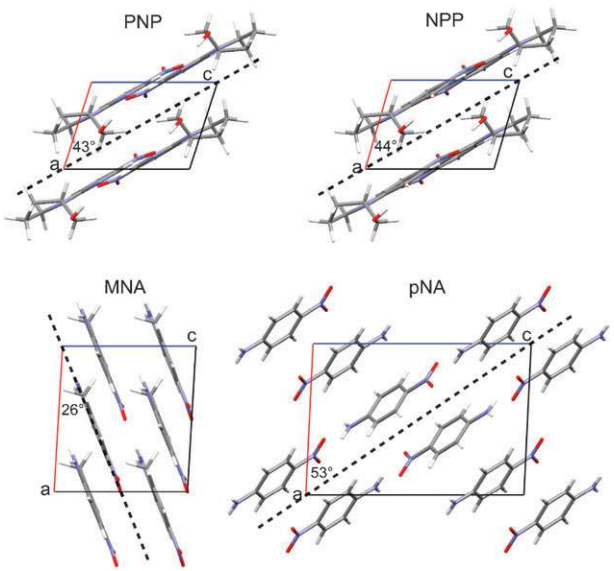

Fig. 2 Cell packing diagrams for the monoclinic crystal structures projected along the *b* axis. The dashed line represents the (101) plane for NPP, PNP and pNA, and the (−102) plane for MNA. Angles (θ, Table 3) are given between these planes and the *a* axis.

for n_Y and n_Z are 6%–7% below the experimental measurements at 1064 nm for NPP[35] and 7–8% for PNP,[36] and the result for n_X is within ~1% in both cases. For these isostructural crystals the principal index n_Y lies along the cell *b* axis, but the directions corresponding to n_X and n_Z are not determined by space group symmetry (although they must lie in the *ac* plane). We see that all results consisently predict the angle θ between n_Z and the *a* axis to be 42–43° for NPP and 40–41° for PNP. This is perhaps unsurprising, as they are essentially the same as the values of 44 and 43°, respectively, which are the angles between the (101) plane and the *ab* plane. From Fig. 2 it is clear that the molecules in both NPP and PNP pack along this direction, which is a natural cleavage plane. Although the available experimental evidence is limited, for both NPP and PNP it suggests that the optic axis corresponding to the largest refactive index is within a few degrees of the (101) plane.[36,43]

3.4.5 pNA. Electron correlation increases the principal refractive indices by 2–5%, a similar result to that found for NPP and PNP. However, in contrast with all previous examples, the Lorentz field leads to a substantial increase of 5% for n_Z, the largest principal refractivity; changes in the other principal values are much smaller. This large effect for n_Z compared with previous examples is due to the combination of a larger Lorentz field (Table 2) coupled with a greater polarizability in the direction of the field, directly in line with the prediction from eqn (2). The main features of the dielectric tensor predicted at the MP2 + field level are faithfully reproduced by the XCHF results. Experimental measurements of various principal refractive indices are available, but they appear to comprise two sets of conflicting values, especially for the largest component, n_Z. Lasheen and Ibrahim[37] reported measurements at 588 nm, and clearly identified the value of 1.756(3) with the *b* axis, but did not indicate directions for the other two components. The assignment in Table 3 is based on their relative magnitudes and, based on comparison of *ab initio* and XCHF results for the other molecules, the value of n_Z reported by Lasheen and Ibrahim seems much too low and is likely to be in error. In other work, Winchell[44] reports measurements attributed to Groth:[45] "(+?)$2V$ = about 80°, $N_X' = 1.556$, $N_Y > 1.78$, N_Z = ?". As recognised by Tanaka,[38] these observations can be used to deduce two possible values for N_Z by assuming either choice of sign for the optic angle $2V$. The relevant expressions[33] yield $N_Z = 2.38$ (assuming $+2V$) and 2.01 (assuming $-2V$). Tanaka adopted the value corresponding to the negative sign, and we see from Table 3 that this choice is also consistent with our present XCHF and MP2 + field results.

As observed for NPP and PNP, the angle θ between the direction corresponding to n_Z and the *a* axis is very close to the angle of 53° between the *ab* plane and the crystallographic (101) plane, which is also a cleavage plane for this material[38] (see also Fig. 2).

3.4.6 MNA. The trend in *ab initio* results for MNA is broadly similar to that observed for pNA, namely increases in the range 1%–5% with inclusion of electron correlation, and a substantial increase (7% in this case) in the largest principal refractivity. This can also be rationalized on the basis of the larger Lorentz field coupled with an even larger molecular polarizability along the direction of the field. Two sets of experimental measurements are available for MNA, and the inconsistencies between them have been previously noted by us.[2] Our previous work using an empirical approach as well as a scaling procedure did not favour one set of results over the

Table 4 Agreement indices for comparison of HF, MP2 and MP2 + field refractive indices with XCHF results

		HF	MP2	MP2 + field
Benzene	Δ^a	0.021	0.012	
	$\%\Delta^b$	1.3	0.8	
Urea	Δ	0.068	−0.001	0.003
	$\%\Delta$	4.5	0.0	0.2
POM	Δ	0.029	−0.031	−0.026
	$\%\Delta$	1.7	−1.9	−1.6
NPP	Δ	0.053	−0.005	−0.013
	$\%\Delta$	3.2	−0.3	−0.7
PNP	Δ	0.013	−0.052	−0.057
	$\%\Delta$	0.8	−3.2	−3.5
pNA	Δ	0.078	0.028	−0.009
	$\%\Delta$	4.0	1.1	−0.8
MNA	Δ	0.049	−0.005	−0.051
	$\%\Delta$	3.0	−0.1	−2.6
Overall	Δ	0.036	−0.007	−0.022
	$\%\Delta$	2.6	−0.5	−1.5

[a] Mean deviation, *e.g.* $\Delta(\mathrm{HF}) = \sum_{i=1,3} [n_i(\mathrm{XCHF}) - n_i(\mathrm{HF})]$. [b] Mean percent deviation, *e.g.* $\%\Delta(\mathrm{HF}) = 100 \sum_{i=1,3} [(n_i(\mathrm{XCHF}) - n_i(\mathrm{HF}))/n_i(\mathrm{XCHF})]$.

other. Here we see quite clearly that the MP2 + field results agree well with the measurements of Grossman and Garito,[39] strongly suggesting that the earlier measurements by Morita *et al.*[40] suffer from a systematic error of some kind. On the other hand, the earlier measurements made by Levine *et al.* of n_Z (2.2 at 532 nm, 2.0 ± 0.1 at 632.8 nm and 1.8 at 1064 nm) and n_Y (1.6 ± 0.1 at 632.8 nm) are in accord with those of Morita *et al.* For the optic axis inclination associated with n_Z we obtain a value of 28° from the *a* axis, which is clearly determined by the arrangement of molecules in the crystal (Fig. 2), and is close to the value of 26° for the (−102) plane; this is also known to be an easy cleavage plane.[46] The experimental determination of this direction by Lipscomb *et al.*[46] suggests a greater angle by as much as 8°, but with actual values very dependent on the crystal sample.

3.4.7 Overall trends. Table 4 summarizes the overall agreement between HF, MP2 and MP2 + field refractive indices and XCHF results obtained by wavefunction fitting. Two simple statistics are provided: the mean deviation, Δ, and mean percentage deviation, %Δ. Although results vary considerably between systems, a relatively robust overall trend can be discerned: *ab initio* calculations at the HF level underestimate XCHF results, typically by several percent (or ~0.03 to 0.05 in any n_i), MP2 results are in remarkably good agreement with XCHF values, and if anything slightly overestimate the XCHF results, while the addition of a Lorentz field appears to generally overestimate the effect of the crystal field.

4. Numerical aspects of the procedure

The *ab initio* calculations (HF, MP2, MP2 + field) reported here are relatively straightforward, and can be performed in commercially available packages. The constrained wavefunction procedure is new and its numerical convergence and robustness properties are briefly discussed here.

The constrained wavefunction procedure is not as straightforward as the other *ab initio* techniques. We have observed that the use of diffuse DZP + basis sets necessary for obtaining good polarizabilities makes the convergence of the X-ray constrained wavefunction harder: more iterations are required relative to using standard basis sets. We have traced some of these convergence problems to near-linear dependencies in the DZP + basis sets, which were particularly severe in the case of MNA, where linear combinations of basis functions corresponding to overlap matrix eigenvalues less than 10^{-5} were removed (by projection) from the basis set expansion of the molecular orbitals, and in the Fock matrix they were explicitly decoupled and shifted to very high energy using level-shifting techniques.[47] With these linear dependencies removed, the SCF convergence was improved, or made possible where previously it was not possible. Nevertheless, the process remains relatively time-consuming relative to when standard (non-diffuse) basis sets are used.

A second complication with the constrained wavefunction procedure arises because the termination criterion for fitting was set to be when $R_w(F)$ approached that of a multipole refinement. Thus, in the scheme used here, a multipole refinement was necessary before the constrained wavefunction procedure was applied. In fact, in many of the cases examined here the constrained wavefunction procedure was very close to the limit of its convergence, *i.e.* the procedure was: (i) taking nearly 50 or more SCF iterations to converge, even with extrapolation techniques applied; (ii) the error in the trial molecular orbitals was not clearly monotonically decreasing toward the end of the SCF procedure; and (iii) the improvement in χ^2 and other agreement statistics was minimal with increases in the lambda parameter. Thus, terminating the X-ray constrained wavefunction fitting procedure at the multipole-refined value of R_w amounts to much the same thing as termination at the limit of what was numerically possible in the constrained wavefunction fitting procedure.

The fact that the constrained wavefunctions generally could not improve upon the multipole R_w may possibly be attributed to the fact that the geometric and ADP parameters used for the constrained wavefunction calculations were obtained from the corresponding multipole refinements. A lower R_w for the constrained wavefunction could possibly be obtained by performing a Hirshfeld-atom refinement on the unconstrained wavefunction, before performing a constrained wavefunction refinement.[48] Thus, in some sense, the constrained wavefunction may be using electronic distortions in the wavefunction to model sub-optimal positional and ADP parameters that result from the multipole model, and it could be argued that the multipole model restricts the ability of the constrained wavefunction to obtain lower R_w values. Nevertheless, we have chosen to use a consistent set of multipole-derived parameters in this work to facilitate comparison.

There also remains a question about the robustness of the results obtained from the constrained wavefunction procedure. For example, how might the results vary if fitting is performed on a different set of X-ray structure factors for the same material? In the process of investigating the convergence problems for MNA we measured another charge density data set on a new crystal. The quality of the new data was similar to that used above. The molecular dipole moment obtained was 9.89 D, compared with a value of 9.20 D reported in Table 2. Principal refractive indices of 1.40, 1.62 and 1.85 compare reasonably well with values of 1.46, 1.66 and 1.85 in Table 3. We see that refractive indices obtained from the two different X-ray data sets are within ~4% of one another, while the estimate of the in-crystal dipole moment is somewhat less robust.

One may also ask about the basis set dependence of the results. The DZP + basis set used here has a particularly diffuse H atom polarization function, with exponent 0.1 au, one-tenth of the next smallest basis function. By re-fitting the new X-ray data for MNA to a level R_w = 1.6% using a modified basis set (where the most diffuse H basis functions were replaced with exponents of 0.25 au) the dipole moment obtained was 9.13 D. This is certainly different from the value of 9.89 D obtained with the more diffuse basis set, and fortuitously close to the result reported in Table 2, and obtained with the more diffuse basis set. The variability of the dipole moment obtained with changes in diffuse basis function exponents appears to be of the same order of magnitude as that obtained by using a different set of X-ray data, and it amounts to ~0.7 D in this case. Refractive indices

obtained with the modified basis set were 1.40, 1.62, and 1.81, which are close to the results from the original diffuse basis. Again, it appears that the refractive indices are more robust to changes in basis than the dipole moments.

Finally, it is worth commenting on the convergence of the dipole moment and refractive indices with the lambda fitting parameter and with R_w. From the results for the fitting of the original MNA data discussed above:

$\lambda = 0.0$, $R_w = 2.16\%$, $\mu = 8.30$ D, $n_i = (1.413, 1.639, 1.787)$

$\lambda = 0.4$, $R_w = 1.74\%$, $\mu = 8.94$ D, $n_i = (1.422, 1.647, 1.820)$

$\lambda = 1.0$, $R_w = 1.64\%$, $\mu = 9.17$ D, $n_i = (1.441, 1.653, 1.829)$

$\lambda = 2.0$, $R_w = 1.55\%$, $\mu = 9.19$ D, $n_i = (1.460, 1.659, 1.845)$,

we can see that it is straightforward to reduce the R_w to 1.7%. The larger fraction of change in the dipole moment and refractive indices has occurred by this stage. By the time an R_w of 1.6% has been reached the electrical properties from the X-ray constrained wavefunction have essentially converged. It is thus not necessary to achieve exactly the same R_w as obtained in a multipole refinement to achieve reasonable electrical properties, but in order for results to be reproduced it is necessary to quote the values of the agreement statistics at which the fitting procedure is terminated.

5. Concluding remarks

The results presented in this work provide clear evidence that single-determinant wavefunctions constrained to fit X-ray diffraction data reflect genuine effects of intermolecular interactions in crystals. In a very real sense they may be regarded as providing estimates of "in crystal" molecular properties, both one-electron (such as expectation values of the charge density) and response properties (such as polarizabilities). The results for dipole moments are compelling in this regard, as the XCHF values are typically in excellent agreement with MP2 + field *ab initio* estimates. The coupled-perturbed Hartree–Fock approach provides XCHF polarizabilities for molecules without the need for the approximations and scaling procedure introduced in our previous work,[2] and where meaningful comparisons can be made with other measurements (*e.g.*, for benzene) the XCHF polarizability provides better agreement than either HF or MP2 calculations.

An important outcome of this research has been the success of an *ab initio* hierarchy of HF, MP2 and MP2 + field calculations to provide benchmarks against which to compare the XCHF results, and we also note that the XCHF results provide a useful benchmark for the MP2 + field results. This adds further weight to the earlier observation[17] that this simple approach involving a self-consistent calculation of the electric field, and computed using dipole lattice sums, is capable of yielding realistic estimates of the electric field experienced by a molecule in a crystal. This is clearly not always the case: results for POM and MNA suggest that improved estimates of this kind will require a convenient description of the *non-uniform* electric field experienced by the molecule in the crystal.

Our principal goal in this work was to use XCHF polarizabilities to estimate refractive indices (albeit at zero frequency) for molecular crystals. The consistent and sensible agreement of the XCHF results with experimental measurements at optical frequencies (Table 3) confirms that this approach is capable of providing both meaningful results and considerable insight into the relative importance of molecular properties and crystal field effects in determining the detailed nature of the refractivity tensor. But it is also important to recognise that the present refractivities—based on XCHF and *ab initio* wavefunctions—were obtained with the RLFT*n* approximation and the local field theory treatment of Munn and co-workers, and this is not without limitations. And we are again surprised by the relative paucity of experimental information on linear optical properties (in this case the refractive index) for important NLO materials such as pNA and MNA.

The XCHF procedure for polarizabilities and refractive indices is less straightforward to apply than for properties such as the charge density or electric potential mainly because the use of diffuse basis sets necessary for accurate polarizabilities leads to convergence problems in the SCF procedure, a problem which has required special solutions. Nevertheless, when fitting to another X-ray data set of equivalent quality, comparable refractive indices were obtained even though the dipole moment may be sensitively dependent on the diffuse functions used in the basis set.

An important advantage of the current approach to computing XCHF response properties over that used in ref. 2 is that it can be readily extended to treat NLO properties, for which the role of the crystalline environment is expected to be considerable.[6] We have computed the molecular hyperpolarizability tensor, $\boldsymbol{\beta}$, for the molecules considered in the present work, as well as the bulk second-order susceptibility $\boldsymbol{\chi}^{(2)}$, and these results will be described in detail in a subsequent publication.

Acknowledgements

This work has been supported by the Australian Research Council.

References

1 C. Bosshard, R. Spreiter, U. Meier, I. Liakatas, M. Bösch, M. Jäger, S. Manetta, S. Follonier and P. Günter, in *Crystal Engineering: From Molecules and Crystals to Materials*, ed. D. Braga, F. Grepioni and A. G. Orpen, Kluwer Academic, Dordrecht, 1999, pp. 261–278; C. Bosshard, K. Sutter, P. Prêtre, J. Hulliger, M. Flörsheimer, P. Kaatz and P. Günter, *Organic Nonlinear Optical Materials*, Gordon and Breach, Basel, 1995.
2 A. E. Whitten, D. Jayatilaka and M. A. Spackman, *J. Chem. Phys.*, 2006, **125**, 174505.
3 D. A. Dunmur, *Mol. Phys.*, 1972, **23**, 109–115.
4 P. J. Bounds and R. W. Munn, *Chem. Phys.*, 1981, **59**, 47–53.
5 P. G. Cummins, D. A. Dunmur, R. W. Munn and R. J. Newham, *Acta Crystallogr., Sect. A*, 1976, **32**, 847–853.
6 H. Reis, M. G. Papadopoulos, C. Hättig, J. G. Angyan and R. W. Munn, *J. Chem. Phys.*, 2000, **112**, 6161–6172.
7 D. J. Grimwood, I. Bytheway and D. Jayatilaka, *J. Comput. Chem.*, 2003, **24**, 470–483.
8 J. Gerratt and I. M. Mills, *J. Chem. Phys.*, 1968, **49**, 1719–1729.
9 J. Gerratt and I. M. Mills, *J. Chem. Phys.*, 1968, **49**, 1730–1739.

10 R. M. Stevens, R. M. Pitzer and W. N. Lipscomb, *J. Chem. Phys.*, 1963, **38**, 550–560.
11 A. G. Ioannou, S. M. Colwell and R. D. Amos, *Chem. Phys. Lett.*, 1997, **278**, 278–284.
12 A. J. Thakkar, T. Koga, M. Saito and R. E. Hoffmeyer, *Int. J. Quantum Chem., Quantum Chem. Symp.*, 1993, **27**, 343–354.
13 A. E. Whitten and M. A. Spackman, *Acta Crystallogr., Sect. B*, 2006, **62**, 875–888.
14 A. J. Sadlej, *Collect. Czech. Chem. Commun.*, 1988, **53**, 1995–2016.
15 D. J. Grimwood and D. Jayatilaka, *Acta Crystallogr., Sect. A*, 2001, **57**, 87–100.
16 M. J. Frisch, G. W. Trucks, H. B. Schlegel, G. E. Scuseria, M. A. Robb, J. R. Cheeseman, J. A. Montgomery, T. Vreven, K. N. Kudin, J. C. Burant, J. M. Millam, S. S. Iyengar, J. Tomasi, V. Barone, B. Mennucci, M. Cossi, G. Scalmani, N. Rega, G. A. Petersson, H. Nakatsuji, M. Hada, M. Ehara, K. Toyota, R. Fukuda, J. Hasegawa, M. Ishida, T. Nakajima, Y. Honda, O. Kitao, H. Nakai, M. Klene, X. Li, J. E. Knox, H. P. Hratchian, J. B. Cross, V. Bakken, C. Adamo, J. Jaramillo, R. Gomperts, R. E. Stratmann, O. Yazyev, A. J. Austin, R. Cammi, C. Pomelli, J. W. Ochterski, P. Y. Ayala, K. Morokuma, G. A. Voth, P. Salvador, J. J. Dannenberg, V. G. Zakrzewski, S. Dapprich, A. D. Daniels, M. C. Strain, O. Farkas, D. K. Malick, A. D. Rabuck, K. Raghavachari, J. B. Foresman, J. V. Ortiz, Q. Cui, A. G. Baboul, S. Clifford, J. Cioslowski, B. B. Stefanov, G. Liu, A. Liashenko, P. Piskorz, I. Komaromi, R. L. Martin, D. J. Fox, T. Keith, M. A. Al-Laham, C. Y. Peng, A. Nanayakkara, M. Challacombe, P. M. W. Gill, B. Johnson, W. Chen, M. W. Wong, C. Gonzalez and J. A. Pople, *GAUSSIAN 03 (Revision C.02)*, Gaussian, Inc., Wallingford, CT, 2004.
17 M. A. Spackman, P. Munshi and D. Jayatilaka, *Chem. Phys. Lett.*, 2007, **443**, 87–91.
18 M. A. Spackman, P. Munshi and B. Dittrich, *ChemPhysChem*, 2007, **8**, 2051–2063.
19 H. Reis, M. G. Papadopoulos and R. W. Munn, *J. Chem. Phys.*, 1998, **109**, 6828–6838.
20 R. D. Brown, P. D. Godfrey and J. Storey, *J. Mol. Spectrosc.*, 1975, **58**, 445–450.
21 H. Birkedal, D. Madsen, R. H. Mathiesen, K. Knudsen, H. P. Weber, P. Pattison and D. Schwarzenbach, *Acta Crystallogr., Sect. A*, 2004, **60**, 371–381.
22 G. S. Chen, C. S. Liu, R. Glaser and J. F. Kauffman, *Chem. Commun.*, 1996, 1719–1720.
23 A. Fort, J. Muller, O. Cregut, J. P. Vola and M. Barzoukas, *Opt. Mater.*, 1998, **9**, 271–275.
24 C. Bosshard, G. Knöpfle, P. Pretre and P. Günter, *J. Appl. Phys.*, 1992, **71**, 1594–1605.
25 L. T. Cheng, W. Tam, S. H. Stevenson, G. R. Meredith, G. Rikken and S. R. Marder, *J. Phys. Chem.*, 1991, **95**, 10631–10643.
26 C. S. Liu and J. F. Kauffman, *Rev. Sci. Instrum.*, 1996, **67**, 525–529.
27 K. L. Kott, C. M. Whitaker and R. J. McMahon, *Chem. Mater.*, 1995, **7**, 426–439.
28 E. M. Breitung, W. E. Vaughan and R. J. McMahon, *Rev. Sci. Instrum.*, 2000, **71**, 224–227.
29 J. W. Smith and S. M. Walshaw, *J. Chem. Soc.*, 1957, 4527–4531.
30 G. L. D. Ritchie and J. N. Watson, *Chem. Phys. Lett.*, 2000, **322**, 143–148.
31 R. Gay and B. Lemanceau, *Cahiers Phys.*, 1956, **74**, 38–40.
32 J. M. Halbout, S. Blit, W. Donaldson and C. L. Tang, *IEEE J. Quantum Electron.*, 1979, **15**, 1176–1180.
33 E. E. Wahlstrom, *Optical Crystallography*, Wiley, New York, 1979.
34 J. Zyss, D. S. Chemla and J. F. Nicoud, *J. Chem. Phys.*, 1981, **74**, 4800–4811.
35 I. Ledoux, C. Lepers, A. Périgaud, J. Badan and J. Zyss, *Opt. Commun.*, 1990, **80**, 149–154.
36 K. Sutter, C. Bosshard, W. S. Wang, G. Surmely and P. Günter, *Appl. Phys. Lett.*, 1988, **53**, 1779–1781.
37 M. A. Lasheen and I. H. Ibrahim, *Acta Crystallogr., Sect. A*, 1975, **31**, 136–141.
38 J. Tanaka, *Bull. Chem. Soc. Jpn.*, 1963, **36**, 833–847.
39 C. H. Grossman and A. F. Garito, *Mol. Cryst. Liq. Cryst.*, 1989, **168**, 255–267.
40 R. Morita, N. Ogasawara, S. Umegaki and R. Ito, *Jpn. J. Appl. Phys.*, 1987, **26**, L1711–L1713.
41 K. Betzler, H. Hesse and P. Loose, *J. Mol. Struct.*, 1978, **17**, 393–396.
42 M. Guillaume, E. Botek, B. Champagne, F. Castet and L. Ducasse, *J. Chem. Phys.*, 2004, **121**, 7390–7400.
43 J. Zyss, J. F. Nicoud and M. Coquillay, *J. Chem. Phys.*, 1984, **81**, 4160–4167.
44 A. N. Winchell, *Optical Properties of Organic Compounds*, University of Wisconsin Press, Madison, 1943.
45 P. Groth, *Chemische Kristallographie*, W. Engelmann, Leipzig, 1917.
46 G. F. Lipscomb, A. F. Garito and R. S. Nerang, *J. Chem. Phys.*, 1981, **75**, 1509–1516.
47 V. R. Saunders and I. H. Hillier, *Int. J. Quantum Chem.*, 1973, **7**, 699–705.
48 D. Jayatilaka and B. Dittrich, *Acta Crystallogr., Sect. A*, 2008, **64**, 383–393.

